Supporting Information

Zhang et al. 10.1073/pnas.1410533111

SI Materials and Methods

Cell Culture, Plasmids, and Pharmacological Inhibition. Both cell lines were maintained at 37 °C with 5% (vol/vol) CO_2, with retinal pigment epithelial cells (RPE-1 cells) in DMEM/F12 (Life Technologies) supplemented with 10% (vol/vol) FBS (HyClone Laboratories), and NIH 3T3 cells in DMEM (Life Technologies) supplemented with 10% (vol/vol) donor adult bovine serum (HyClone Laboratories). Both media were supplemented with 2 mM L-glutamine, 100 μg/mL streptomycin, and 100 U/mL penicillin (Life Technologies).

Red fluorescent protein (RFP)-zyxin was constructed by recloning the enhanced green fluorescent protein (EGFP) construct (1) into the pDsRed1-N1vector (Clontech). EGFP-tagged paxillin (1) were kindly provided by Dr. Juergen Wehland (Deutsche Forschungsgemeinschaft, Braunschweig, Germany).

Cells were treated with 2 μM (for RPE-1 cells) or 5 μM (for NIH 3T3 cells) nocodazole (Sigma-Aldrich) to induce microtubule depolymerization, or 5 μM Taxol (Sigma-Aldrich) to stabilize microtubules. Myosin activity was inhibited by adding in 50 μM blebbistatin (Calbiochem). Cells were treated with 50 μM ciliobrevin D (Xcess Biosciences) to inhibit cytoplasmic dynein.

Live-Cell Imaging, Immunofluorescence Staining. For migration analysis, phase-contrast images of migrating cells were collected with a Nikon Eclipse Ti microscope using a 10× PlanFluor dry objective. For quantification of focal adhesion proteins, phase-contrast and fluorescent images were collected with a 40× PlanFluor dry objective. Images were collected every 4 min for a period up to 24 h. To avoid the complication of cell–cell interactions on migration, only single cells were analyzed.

Immunofluorescence images were acquired by fixing the cells with 4% (wt/vol) formaldehyde (Thermo Scientific) in PBS and staining with antibodies against vinculin (Santa Cruz Biotechnology) or tensin (Sigma-Aldrich).

Micropatterning Using Linear Polyacrylamide. Linear polyacrylamide-blocked micropatterns were prepared as described previously (2). Briefly, coverslips were activated with Bind-Silane (Sigma-Aldrich), and areas for cell adhesion were covered selectively with positive photoresist SPR-220 (MicroChem) through UV exposure, baking, and development. The remaining area is made nonadhesive by grafting linear polyacrylamide to the Bind-Silane–activated glass surface. The photoresist-protected adhesive region is then exposed by stripping off the photoresist. Some of the micropatterned substrates were incubated for 30 min with 20 μg/mL fibronectin (Sigma-Aldrich) with or without the conjugation of Alexa Fluor 568 dye (Invitrogen). Unless otherwise specified, the pattern consisted of a variety of strips 4–24 μm in width. Some experiments were performed with uniform strips 10 μm in width.

Image Analysis. Image processing was carried out using ImageJ (National Institutes of Health, Bethesda, MD), Matlab (MathWorks), and a custom software.

For the quantification of front-to-rear focal adhesion density ratio, the outline of a cell and its nucleus was first obtained by manual segmentation of a phase-contrast image. The outline was then used to determine the centroids of the cell and the nucleus, which were then used to determine the transient direction of cell migration. A straight line through the cell nucleus perpendicular to the migration direction was then used to separate the cells into front and rear regions. Total focal adhesion protein area was quantified by first thresholding the fluorescent image of focal adhesions, then summing the area of individual focal adhesions over the front and rear region, respectively. To normalize against the different front and rear areas, the total focal adhesion protein area in the front and rear was divided by the area of the front and rear to obtain the front and rear focal adhesion protein density, respectively. Finally, front and rear protein densities are used to calculate the front-to-rear ratio, r. If the calculated value is larger than 1, its inverse is used instead, which may happen for cells about to switch directions. This procedure ensured that any less than perfectly uniform distribution of focal adhesion protein would yield a value smaller than 1. We took [1 – min (r, 1/r)] as the index of polarization—a perfectly uniform localization would result in an index of 0.

The quantification of time-averaged cell length and oscillation period is done either manually using ImageJ by processing the kymographs or automatically with a custom Matlab code. Persistence is given as a ratio of net migration distance divided by the total path length, and is calculated with our custom software.

Statistical Analysis. The data are analyzed statistically by independent/paired two-tailed Student t test, ANOVA, ANCOVA, χ^2 test, or Fisher's exact test. Data are presented in a mean ± SD manner.

Computer Simulation. We have simplified the 2D LEGI model described by Satulovsky et al. (3), by forcing cells to be a very narrow rectangle while maintaining other assumptions described previously. Cell geometry was represented with linear coordinates, rather than 2D polar coordinates as in the previous study. However, to maintain some consistency, cell perimeter was represented by 360 points equally spaced along the two long edges of the rectangle (Fig. S6). In addition, signals along the two long edges were assumed to be the same, due to the narrow width of the cell. Protrusion was allowed only at the two ends along the direction of the strip. The origin of the linear coordinate system was set at the middle of the rectangle, such that the coordinate x for the position may be either positive or negative. This differed from the previous polar coordinate system where x was the distance from the center and was always positive. The position of the cell center was then tracked relative to a fixed origin for the calculation of cell migration and generation of kymographs.

The rule-based model did not involve any specific molecules (3, 4). The conceptual excitation and inhibitory signals may represent either a single molecular entity or a combined effect of multiple signal molecules. The control equation for the excitation signal is similar to that described previously (3). However, instead of forcing the inhibitory signal to be uniform across the cell, we allowed it to diffuse away from the source in a way similar to excitation signals except for a much larger diffusion coefficient. This modification had no effect on the qualitative outcome of the LEGI model (3, 5, 6).

At a given location x and time t, the excitation signal, $S^+(x,t)$, was controlled by the generation from random burst, g, and a positive feedback, f^+, as well as diffusion-like transport process, D^+, and decay of the signal, $-\delta$ (3). The inhibitory signal, $S^-(x,t)$, was controlled by a similar set of parameters, f^-, D^-, $-\delta$, except that there was no random burst of inhibitory signal and that the generation of inhibitory signal was driven by net signals lagged by a time, τ. The control equations are shown below, where $S(x,t) = S^+(x,t) - S^-(x,t)$ was the net signal:

$$\frac{\partial S^+(x,t)}{\partial t} = -\delta\, S^+(x,t) + \max\big(Gaussian(g),0\big) + D^+\nabla^2 S^+(x,t) + f^+ S(x,t), \quad \textbf{[S1]}$$

$$\frac{\partial S^-(x,t)}{\partial t} = -\delta\, S^-(x,t) + D^-\nabla^2 S^-(x,t) + f^- S(x,t-\tau), \quad \textbf{[S2]}$$

where ∇ represents spatial gradient and $f^- = f^+ = 0$ in regions where $S(x,t) \le 0$. $Gaussian(g)$ is a Gaussian distribution with an average of g and a variance equal to the value of g. As stated earlier, g is the average size of random burst per unit time interval, which remains constant across the cell and throughout a given simulation.

Subtracting Eq. **S2** from Eq. **S1**, one obtained a simpler control equation of the net signal $S(x,t)$:

$$\frac{\partial\, S(x,t)}{\partial t} = -\delta\, S(x,t) + \max\big(Gaussian(g),0\big) + D\nabla^2 S(x,t) + f^+ S(x,t) - f^- S(x,t-\tau). \quad \textbf{[S3]}$$

Assuming that the transportation of the inhibitory signals is inhibited upon the disassembly of microtubules, $D^-_{nocodazole} \approx D^+ = D \ll D^-_{control}$ for nocodazole-treated cells.

Delay differential equations are capable of generating oscillations. We found that a delay τ in order of tens of seconds (7, 8) can induce oscillation with a period in the order of tens of minutes, which matched the scale found in the experiments. However, we recognized that this represented a simplification of how a delay and/or limited rate of the generation of inhibitory signals may induce oscillations in a LEGI model.

Simulation of cell shape changes and cell migration were performed as described before (3), but simplified for 1D as follows:

$$\begin{cases} \dfrac{\partial |x_e|}{\partial t} = \max\big([l - l_{min}]R, 0\big), \text{ where } S(x_e,t) < 0, \\ \dfrac{\partial |x_e|}{\partial t} = \max\big(Gaussian(P),0\big), \text{ where } S(x_e,t) > 0, \\ l = x_r - x_l, \end{cases} \quad \textbf{[S4]}$$

where l was the length of the cell, l_{min} was the minimum length of the cell due to incompressible central region including the nucleus. $x_e (e = r, l)$ were the points representing the right and left end of the cell, respectively. P was the average protrusion distance per unit time interval, with a dimension of length/time. R was the distance fraction of retraction per unit time interval, with a dimension of 1/time. These parameters were used to control the distance of protrusion and retraction, hence the length of the cell in a simplified manner. The positions of other membrane points were then determined by spacing them evenly across the length of the cell (Fig. S6).

We found that, without further feedback regulation, control cells may expand indefinitely due to a strong positive feedback of the LEGI mechanism. Infinite expansion was prevented by a simple process that down-regulates the excitation signal as the cell expands in area. Thus, following the determination of cell shape (length) at each time step, the concentration of the excitation signal, $S^+(x)$, is rescaled according to the updated cell area. Because cell width is a constant, the equation becomes the following:

$$S^+_{after}(x) = S^+_{before}(x) \times \frac{l_{before}}{l_{after}}. \quad \textbf{[S5]}$$

The subscript *before*/*after* indicates the value before and after the update at each time step, respectively. An alternative regulation process, implemented previously with a similar outcome, involves the increase of inhibitory signals in proportion to the cell spreading area to enhance retraction during cell spreading (3).

As the intensity of any molecular-based cellular signals cannot go to infinity, we imposed an upper limit value for S^+ and S^- as 1,000 arbitrary units, which is a simplified representation of the saturation concentration of the signals. The limit has no effect on the conditions leading to oscillations, because both signals remain much lower than the limit, neither is it necessary for obtaining persistent migration. However, the cap facilitates the establishment of a steady state and the transition from persistent migration to oscillation upon the simulated addition of nocodazole (Fig. 4*D*), because otherwise net signals may reach a strongly positive value at the front and a strongly negative value at the rear, creating a very strong polarity and requiring a long time for the values to transition into an oscillation state. In addition, for all of the analysis of $V > 0$ cases, S^+ and S^- never reached the cap value.

Computer Simulation of Ciliobrevin D-Treated Cells. The effects of dynein inhibition on cell migration may be understood if one introduces a separate, dynein-dependent transport process of inhibitory signals into the mathematical model. Eq. **S2** is hence revised to include diffusion and advection, as shown in Eq. **S2S**, where $V = |V|$ is the rate of active transport pointing away from the direction of cell migration:

$$\frac{\partial S^-(x,t)}{\partial t} = -\delta\, S^-(x,t) + D^-\nabla^2 S^-(x,t) + f^- S(x,t-\tau) - \nabla\cdot\{V S^-(x,t)\}. \quad \textbf{[S2S]}$$

Instead of using a large diffusion coefficient, D^-, as used in other studies, the revised model keeps D^- constant at a baseline level. A large advection rate ($V \ge 0.90$) recapitulates persistent cell migration, whereas complete inhibition of advection ($V = 0$) reproduces the oscillation induced by nocodazole treatment, which is equivalent to the simulation using the original Eq. **S2**. In addition, we found that a moderate rate of advection can mimic various effects of ciliobrevin D treatment not obtained using the original Eq. **S2**, supporting the idea that ciliobrevin D partially inhibits retrograde transport of inhibitory signals (Fig. S7*C*).

Parameters used in our model simulations are listed in Table S1.

1. Rottner K, Krause M, Gimona M, Small JV, Wehland J (2001) Zyxin is not colocalized with vasodilator-stimulated phosphoprotein (VASP) at lamellipodial tips and exhibits different dynamics to vinculin, paxillin, and VASP in focal adhesions. *Mol Biol Cell* 12(10):3103–3113.
2. Guo W, Wang Y-L (2011) Micropatterning cell-substrate adhesions using linear polyacrylamide as the blocking agent. *Cold Spring Harb Protoc* 2011(3):prot5582.
3. Satulovsky J, Lui R, Wang YL (2008) Exploring the control circuit of cell migration by mathematical modeling. *Biophys J* 94(9):3671–3683.
4. Levine H, Kessler DA, Rappel W-J (2006) Directional sensing in eukaryotic chemotaxis: A balanced inactivation model. *Proc Natl Acad Sci USA* 103(26):9761–9766.
5. Levchenko A, Iglesias PA (2002) Models of eukaryotic gradient sensing: Application to chemotaxis of amoebae and neutrophils. *Biophys J* 82(1):50–63.
6. Ma L, Janetopoulos C, Yang L, Devreotes PN, Iglesias PA (2004) Two complementary, local excitation, global inhibition mechanisms acting in parallel can explain the chemoattractant-induced regulation of PI(3,4,5)P3 response in dictyostelium cells. *Biophys J* 87(6):3764–3774.
7. Kortholt A, Keizer-Gunnink I, Kataria R, Van Haastert PJM (2013) Ras activation and symmetry breaking during *Dictyostelium* chemotaxis. *J Cell Sci* 126(19):4502–4513.
8. Lee S, Shen Z, Robinson DN, Briggs S, Firtel RA (2010) Involvement of the cytoskeleton in controlling leading-edge function during chemotaxis. *Mol Biol Cell* 21(11):1810–1824.

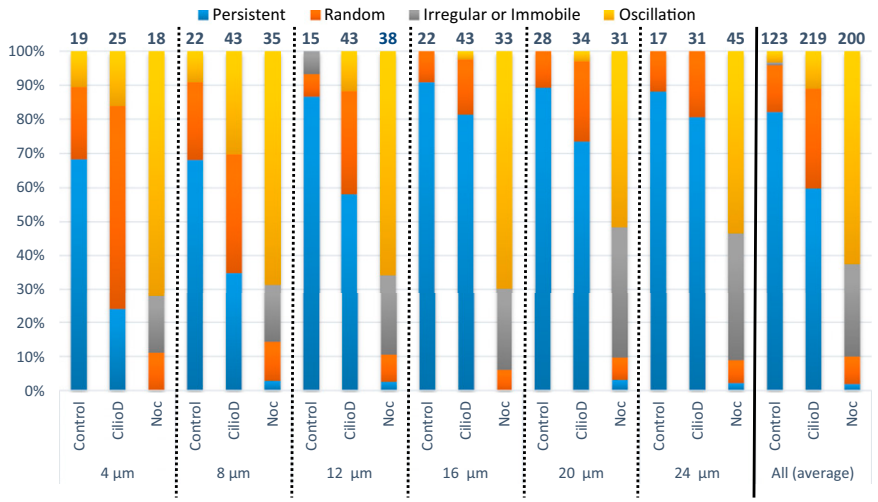

Fig. S1. Cell migratory behavior under different conditions. Related to Figs. 1, 2, and 6. RPE-1 cells on 4- to 24-μm strips with no treatment (Control), treated with 50 μM ciliobrevin D (CilioD) or 2 μM nocodazole (Noc) show different migratory behaviors. Control cells show a high persistence, such that less than 20% of the cells ever changed their migrating directions for at least 5 h. The width of the strip has no apparent effect on the persistent behavior. In contrast, more than 60% of nocodazole-treated cells show oscillatory migration. Ciliobrevin D-treated cells on average show a much higher probability to oscillate than control cells ($P = 0.01$), especially on narrow strips. The total number of cells for each category is listed above each bar (Persistent—unidirectional migrating for ≥5 h; Random—cell changed direction at least once during migration but does not oscillate; Irregular or immobile—cells had no apparent displacement, with or without active protrusion; Oscillation—at least two consecutive cycles of forward-backward movement with a similar amplitude and period). Only single cells are counted; cells immediately before or after division/arrested division are excluded.

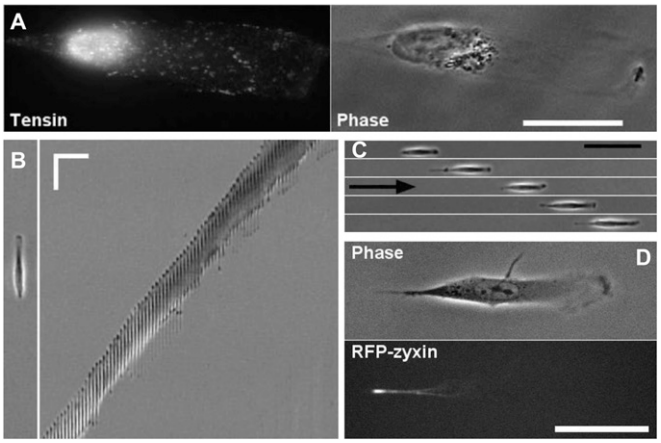

Fig. S2. Persistent migration of cells on 1D strips and the corresponding localization of focal adhesion proteins. Related to Fig. 1. Immunofluorescence staining of tensin in a representative RPE-1 cell (*A*; scale bar, 25 μm) shows no apparent polarization. Kymograph (*B*; scale bar, 50 μm, 60 min) and time series (*C*; 90-min interval; scale bar, 100 μm; arrow indicates the direction of migration) of representative NIH 3T3 fibroblasts exhibiting persistent migration on 1D strips. RFP-zyxin in NIH 3T3 cells migrating on 1D strips localizes to the tail region (*D*). (Scale bar, 50 μm.)

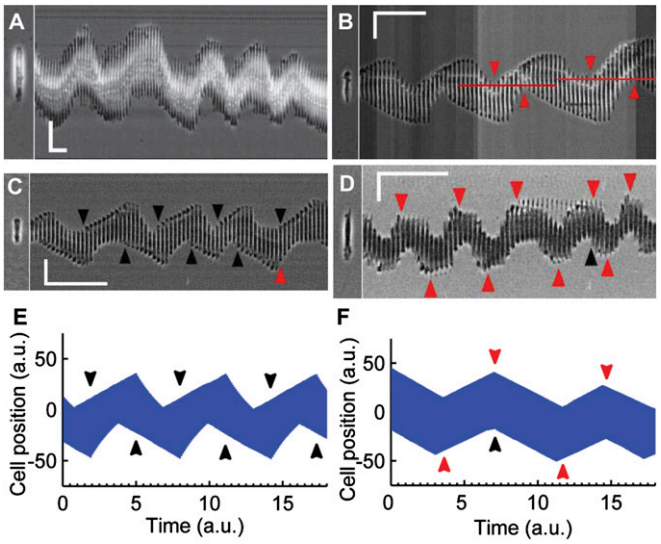

Fig. S3. Cell oscillation on 1D strips induced by nocodazole. Related to Fig. 2. Kymograph of a representative NIH 3T3 cell treated with nocodazole shows oscillatory migration along the strip (*A*). A representative oscillating RPE-1 cell migrates away from the previous locations of adhesion, as indicated by the horizontal lines and arrowheads in the kymograph (*B*). Kymographs of representative RPE-1 cells oscillating on 1D strips and simulated oscillating cells show that the switch of migration direction is initiated mainly by extension of the tail to turn it into a front (*C* and *E*; black arrowheads), but sometimes also by retraction of the front to turn it into a tail (*D* and *F*; red arrowheads). Occasionally, cells switch the direction by simultaneous tail extension and frontal retraction (*C*, *D*, and *F*; paired red and black arrowheads). (Scale bar, 50 μm, 60 min.)

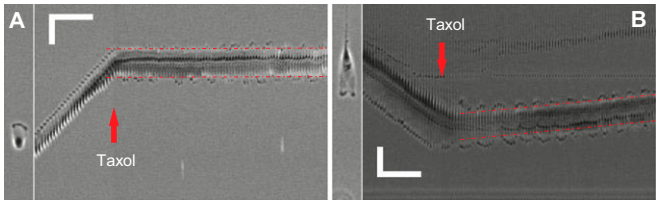

Fig. S4. Effects of Taxol on RPE-1 cell migration. Related to Fig. 2. Kymographs of representative RPE-1 cells treated with Taxol show either an immobile cell body (*A*; representing 36 out of 70 cells) or a slowly drifting cell body (*B*; representing 34 out of 70 cells), with weak protrusion activities at both ends of the cell. Even if the protrusions at the two ends sometimes take place in an alternating manner, similar to the oscillations induced by nocodazole, they are much shorter in distance and the cell body shows hardly any oscillation (as indicated by the dashed lines). (Scale bar, 50 μm, 60 min.)

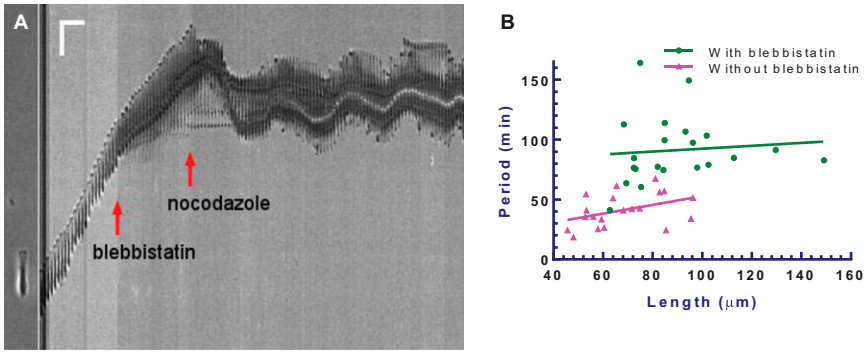

Fig. S5. Effects of myosin II inhibition on the oscillation of RPE-1 cells. Related to Fig. 3. Kymograph shows the migration behavior of a representative RPE-1 cell on a 1D strip treated with blebbistatin, then with nocodazole (*A*). (Scale bar, 50 μm, 60 min.) The increase in oscillation period caused by blebbistatin exceeds that caused by cell length alone (*B*; $n = 21$ for each group, $P < 0.0001$ for ANCOVA test using length as a covariate.)

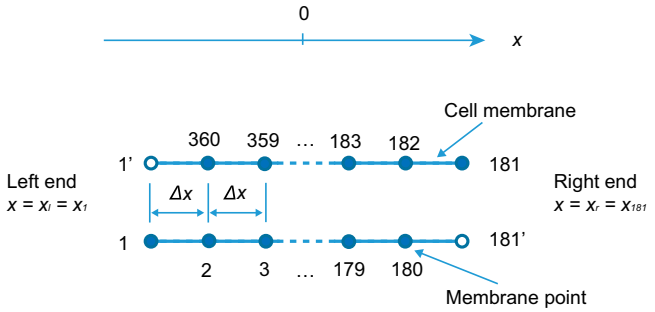

Fig. S6. Illustration of the 1D geometry used in simulation. Related to Fig. 4. A cell migrating on a strip is described as an elongated rectangle. The membrane of the cell is represented by 360 equally spaced points, with the 1st point representing the left end and 181st point representing the right end of the cell. The two ends are allowed to protrude or retract along the *x* axis, according to the sign of local net signals.

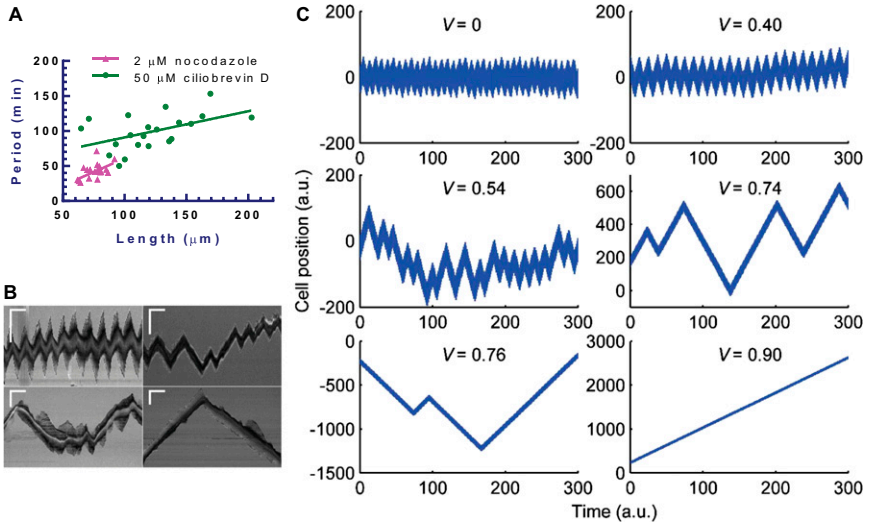

Fig. S7. Oscillation of RPE-1 cells upon the inhibition of dynein. Related to Fig. 6. Oscillating RPE-1 cells show a longer period of oscillation in 50 μM ciliobrevin D than in 2 μM nocodazole, which may be explained by a weak removal of inhibitory signal from the frontal region (*A*; $n = 21$ for ciliobrevin D group and $n = 20$ for nocodazole group; $P < 0.001$ for ANCOVA test using length as a covariate). In addition to stable oscillation with a long period (*B*; *Upper Left*), RPE-1 cells in ciliobrevin D also exhibit migratory behaviors such as transient oscillation (*B*; *Upper Right*), random migration (*B*; *Lower Left*), and weakly persistent migration (*B*; *Lower Right*). Computer simulations indicate that cell migration is strongly dependent on the rate of signal transport (*C*). We assume that microtubule disassembly by nocodazole completely inhibits the transport ($V = 0$; see *Computer Simulation of Ciliobrevin D-Treated Cells* in *SI Materials and Methods*), which facilitates oscillation in contrast to the persistent migration of control cells ($V = 0.90$). The effect of ciliobrevin D may be explained if the dynein inhibitor partially suppresses the transport. Depending on the extent of suppression, the model is able to create stable oscillations with a long period ($V = 0.40$), transient oscillations ($V = 0.54$), random migration ($V = 0.74$), weakly persistent migration ($V = 0.76$), and eventually completely persistent migration similarly to that of control cells. (Scale bar, 100 μm, 120 min.)

Table S1. Parameter values used for simulations

Parameters	Persistent migration* (Movie S4)	Oscillation (Movies S4–S6)	Oscillation in blebbistatin (Movie S6)	Oscillation with different cell lengths (Movie S7)	Oscillation (initiated with frontal retraction)	Slower oscillation in ciliobrevin D	Transient oscillation in ciliobrevin D	Random migration in ciliobrevin D	Persistent migration
l_{min}, [length]	20	20	20	20	20	20	20	20	20
P, [length]/[time]	8	8	8	8	8	8	8	8	8
R, 1/[time]	1/5	1/5	**1/7**[†]	**[1/8.5, 2]**	1/5	1/5	1/5	1/5	1/5
g, [signal]/[time]	10	10	10	10	10	10	10	10	10
D^+, [length]^2/[time]	50	50	50	50	50	50	50	50	50
D^-, [length]^2/[time]	**500**[‡]	50	50	50	10	50	50	50	50
τ[§], [time]	1	1	**1.3**	1	1	1	1	1	1
f^+, 1/[time]	1	1	1	1	1	1	1	1	1
f^-, 1/[time]	1.3	1.3	1.3	1.3	**2**	1.3	1.3	1.3	1.3
δ, 1/[time]	0.1	0.1	0.1	0.1	**0.05**	0.1	0.1	0.1	0.1
V[¶], [length]/[time]	0	0	0	0	0	**0.40**	**0.54**	**0.74, 0.76**	**≥0.90**

*An upper limit of 1,000, which is a simplified representation of the saturation concentration of the signals in random unit, was imposed to the excitation and inhibitory signals, without which these signals tends go to infinity due to the feedback loop. The limit has no effect on the conditions involving oscillations, because both signals remain much lower than the limit.

[†]By adjusting the value of R (from 1/5 to 1/7), we are able to maintain a similar cell length with or without blebbistain treatment, so as to exclude the effect of length change on oscillation period.

[‡]Values in bold indicate a difference from the parameter values used for the simulation of standard oscillation.

[§]The time step used in all the simulations is 0.025.

[¶]$V \neq 0$ is used for the simulation involving the effect of dynein.

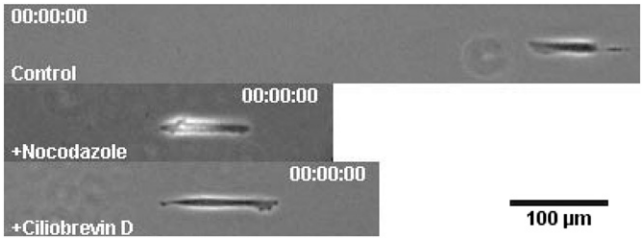

Movie S1. Related to Figs. 1, 2, and 6. Persistent migration and oscillation of RPE-1 cells. The movie shows representative RPE-1 cells migrating persistently as a control or showing oscillations when treated with nocodazole or ciliobrevin D on 1D strips.

Movie S1

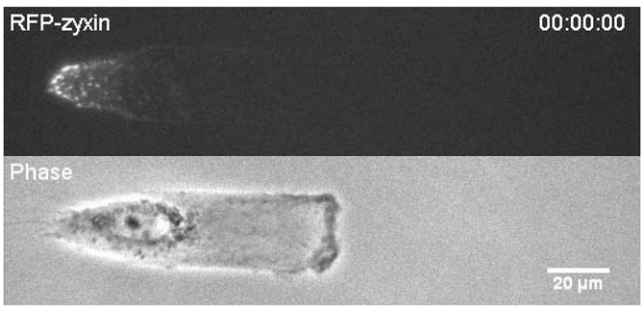

Movie S2. Related to Fig. 2. A representative RPE-1 cell expressing RFP-zyxin and migrating on 1D strip, treated with nocodazole to induce oscillations. The movie shows the redistribution of zyxin upon nocodazole treatment.

Movie S2

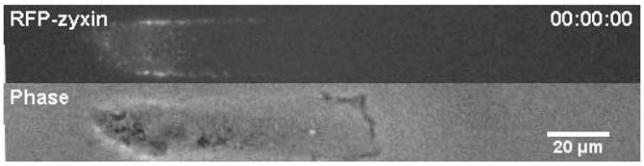

Movie S3. Related to Fig. 3. A representative RPE-1 cell expressing RFP-zyxin and migrating on 1D strip, first treated with nocodazole to induce oscillation, then with blebbistatin to inhibit myosin II. The inhibition of myosin II causes mature focal adhesions to turn into small dot-like focal complexes, and a concomitant increase in the period of oscillation.

Movie S3

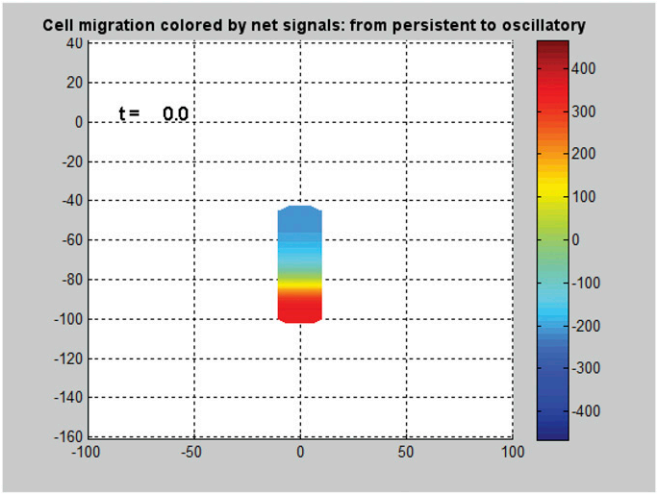

Movie S4. Related to Fig. 4. Computer simulation of a cell migrating persistently in 1D followed by oscillations upon the treatment of nocodazole. The cell is colored to show the heat map of net signals. Red indicates the site of protrusion and blue indicates the site of retraction, which resembles the dynamic distribution of RFP-zyxin.

Movie S4

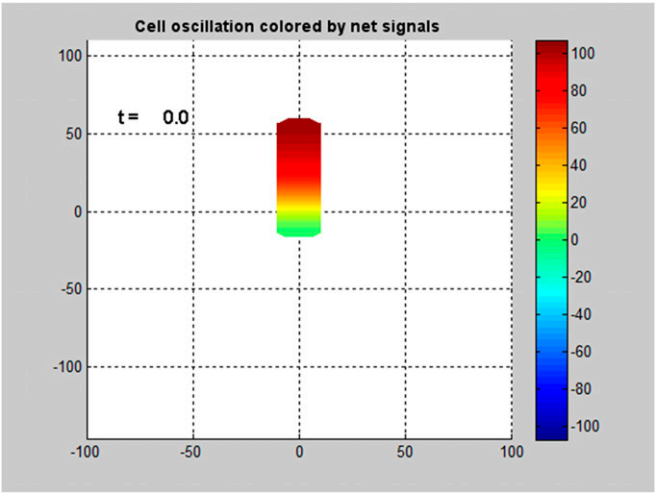

Movie S5. Related to Fig. 4. Computer simulation of a cell oscillating in 1D. The cell is colored to show the heat map of net signals. Red indicates the site of protrusion, and blue indicates the site of retraction.

Movie S5

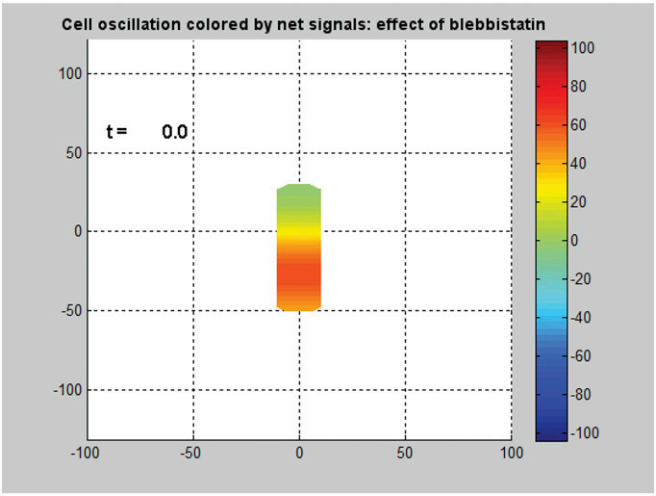

Movie S6. Related to Fig. 4. Computer simulation of an oscillating cell treated with blebbistatin in 1D. The period of oscillation increases as a result of the treatment, even if the cell length is held the same. The cell is colored to show the heat map of net signals. Red indicates the site of protrusion, and blue indicates the site of retraction.

Movie S6

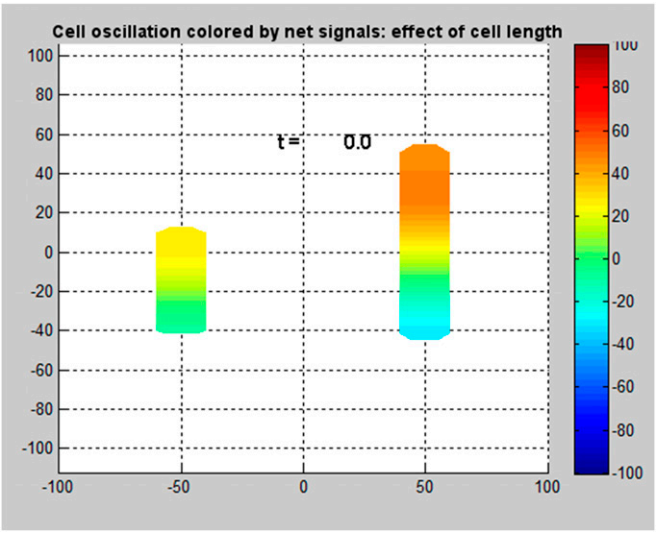

Movie S7. Related to Fig. 5. Computer simulation of the oscillation of a short cell and a long cell. Compared with long cells, short cell shows a faster oscillation and a lower peak signal. The cell is colored to show the heat map of net signals. Red indicates the site of protrusion, and blue indicates the site of retraction.

Movie S7